Supporting Information

Fast one-pot synthesis of Se-rich MnCdSe solid solution for highly efficient cocatalyst-free photocatalytic H_2 evolution

Jieqian Liu[a], Yining Bao[a], Yimin Liu[a], Jingren Yang[b], Toyohisa Fujita[a] and Deqian Zeng[*a]

[a] *Guangxi Key Laboratory of Processing for Non-ferrous Metals and Featured Materials, School of Resources, Environment and Materials, Guangxi University, Nanning 530004, China. E-mail: dqzeng@gxu.edu.cn*

[b] *State Environmental Protection Key Laboratory of Environmental Health Impact Assessment of Emerging Contaminants, Shanghai Academy of Environmental Sciences, Shanghai 200233, China*

Experimental

Preparation of Se-rich MnCdSe nanocrystals

A class of Se-rich MnCdSe solid solutions was prepared through a facile one-pot solution-phase approach. Firstly, anhydrous cadmium chloride ($CdCl_2$) (0.8 mmol, 0.6 mmol, 0.485 mmol, 0.4 mmol), 2.4 mmol of anhydrous manganese chloride ($MnCl_2$), and 3 mmol of selenium (Se) powder were added into 16 mL of oleylamine in a three-neck flask. Then the mixture was heated up to 300℃ for 1 h under an argon atmosphere. The precipitate was cooled down to room temperature and subsequently washed with n-hexane several times. Afterward, the product was collected after drying overnight under a vacuum at 60℃. Similarly, bare CdSe was prepared using the same method without adding $MnCl_2$. Finally, the final product was obtained through a ligand exchange process by exchanging the surface oleylamine with 3-mercaptopropionic acid (MPA), according to previous reports[1, 2].

Characterization

The crystalline phases were studied by an X-ray diffractometer (XRD, Smartlab-3KW (Rigaku Ltd., Japan)). The SEM images were recorded on a scanning electron microscope (SEM, Hitachi SU8220). The TEM images were obtained from a Titan G260-300 transmission electron microscopy. Ultraviolet-visible (UV-vis) diffuse reflectance spectra were obtained from a Lambda-750 spectrometer. X-ray photoelectron spectroscopy (XPS) measurements were identified by a Thermo Fisher Scientific K-Alpha system. Time-resolved photoluminescence (TRPL) spectra (excitation wavelength: 380 nm) were derived from an FL3C-111 (HORIBA Instruments Inc.). The elemental composition of the samples was analyzed by coupled plasma-atomic emission spectroscopy (ICP-AES) using ICPS-7510 (Shimadzu, Japan).

Photocatalytic H_2 evolution tests

The H_2 evolution measurements of the photocatalyst were performed on a sealed Pyrex flask reaction system. In a typical experiment, 30 mg of the photocatalyst was dispersed in 60 mL of 0.35 M Na_2S/0.25 M Na_2SO_3 aqueous solution. Then the mixture was degassed for 30 min by a vacuum pump to remove the dissolved gas. After that, the reactor was vertically irradiated by a 300 W Xe lamp equipped with a 420 nm UV cut-off filter. The generated H_2 was detected by online gas chromatography (GC-7920, N_2 as the carrier gas, TCD). The apparent quantum yield (AQY) was measured using a 420 nm band-pass filter according to the following equation.

$$\mathbf{AQY}\ (\%) = \frac{\mathbf{number\ of\ evolved\ hydrogen\ molecules \times 2}}{\mathbf{number\ of\ incident\ photons}} \times \mathbf{100}\%$$

Photoelectrochemical measurements

The photoelectrochemical (PEC) measurements were conducted on a VSP-300 (Biologic) electrochemical workstation. The working electrodes were prepared as follows: the photocatalyst (5 mg) was dissolved in ethanol (0.5 mL) containing Nafion (10 μL) and ultrasonicated for three hours. Then the ink was deposited on a 2.0 cm^2 ITO glass. The Ag/AgCl (3.5 M KCl) electrode, Pt sheet, and 0.1 M Na_2SO_4 solution served as the reference electrode, counter electrode, and electrolyte, respectively. The photocurrent responses were tested under several visible-light on-off cycles at an applied potential of 0.2 V vs. Ag/AgCl. Electrochemical impedance spectroscopy (EIS) was measured over a frequency range from 10^{-1} to 10^5 Hz. Mott-Schottky plots were determined at frequencies of 500, 1000, and 1500 Hz.

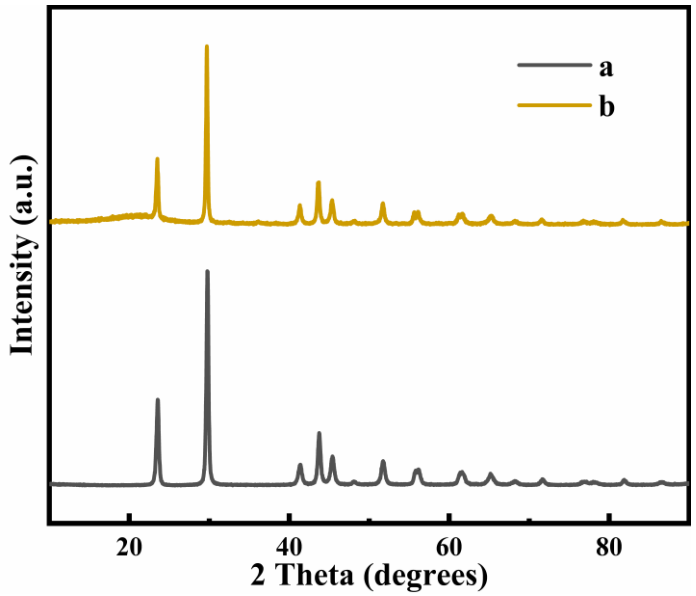

Fig. S1. XRD patterns of Se source (a) and the as-obtained product without adding $CdCl_2$ precursor in the reaction solution (b).

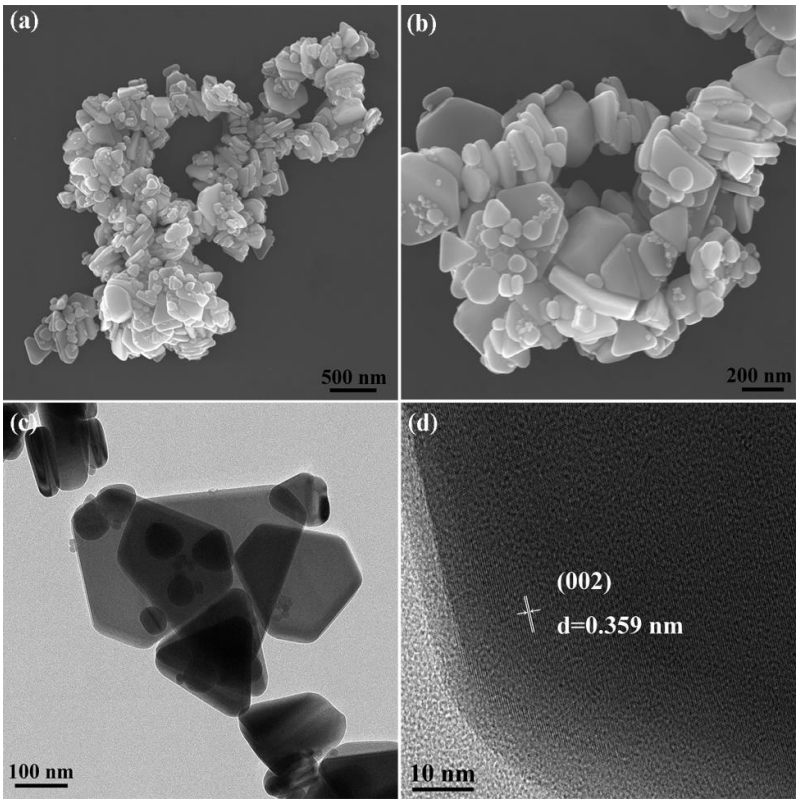

Fig. S2. (a, b) SEM, (c) TEM, and (d) HRTEM images of pure CdSe.

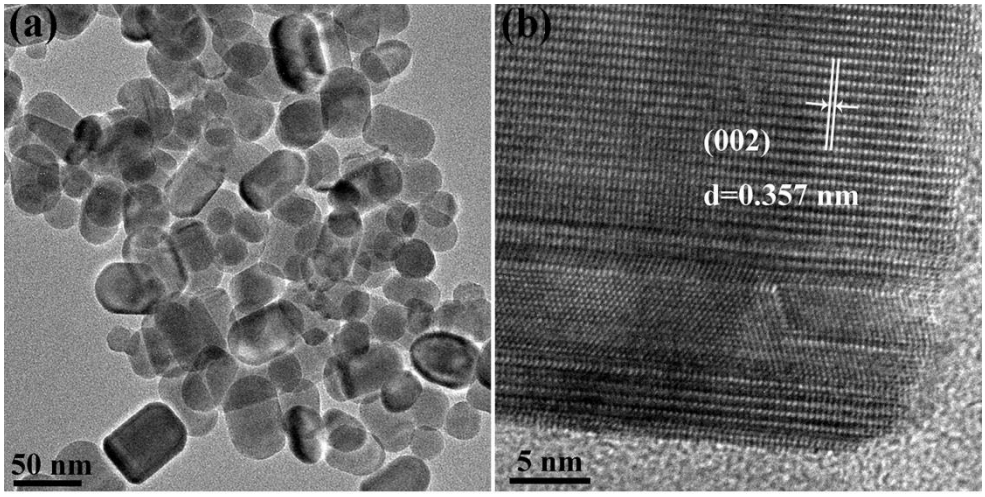

Fig. S3. (a) TEM and (b) HRTEM images of $Mn_{0.33}Cd_{0.67}Se_{1+x}$.

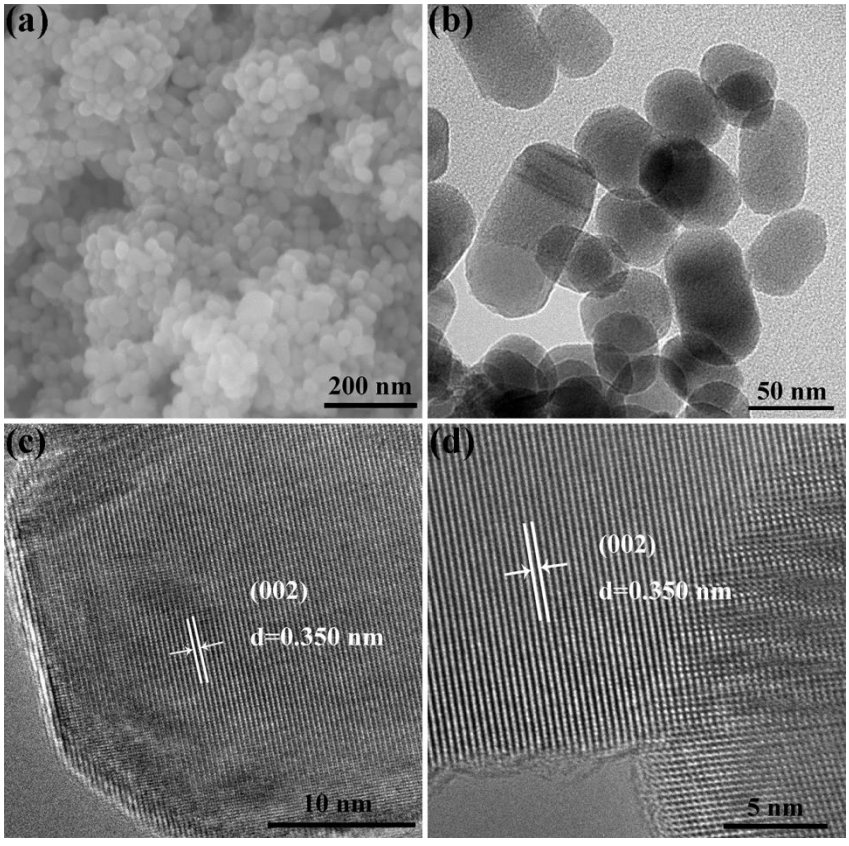

Fig. S4. (a) SEM, (b) TEM, and (c, d) HRTEM images of $Mn_{0.46}Cd_{0.54}Se_{1+x}$.

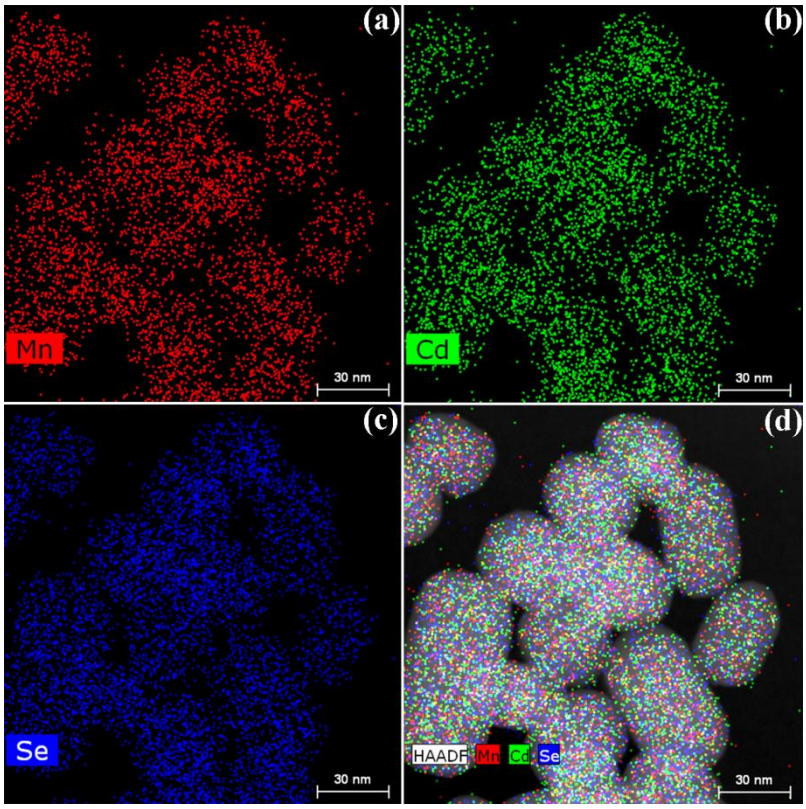

Fig. S5. Elemental mapping images of (a) Mn, (b) Cd, (c) Se, and (d) the corresponding overlapping image of Mn (red), Cd (green), and Se (blue) for $Mn_{0.46}Cd_{0.54}Se_{1+x}$.

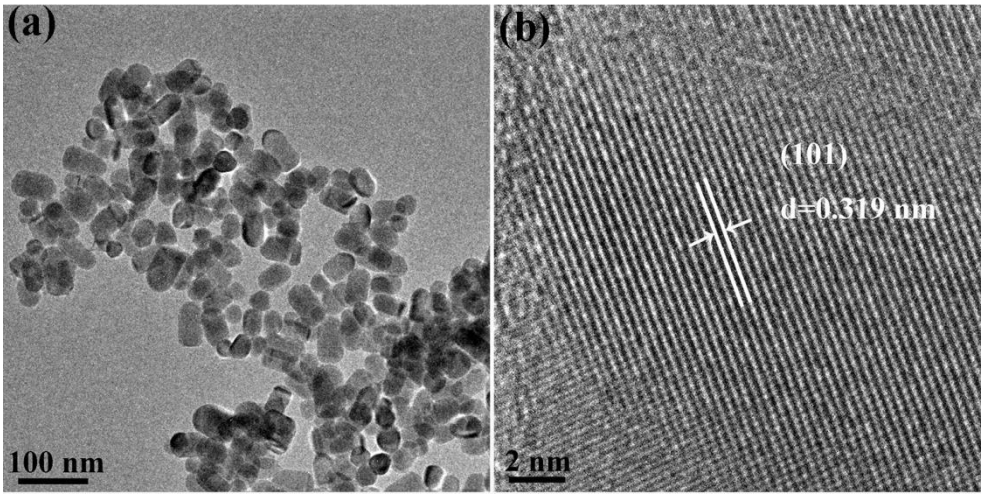

Fig. S6. (a) TEM and (b) HRTEM images of $Mn_{0.70}Cd_{0.30}Se_{1+x}$.

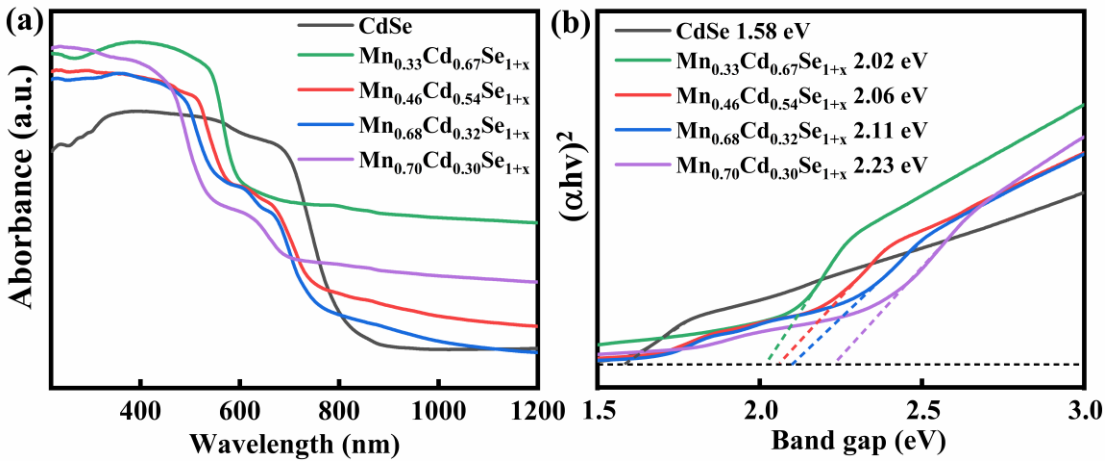

Fig. S7. (a) UV-vis diffuse reflectance spectra and (b) Tauc plots of pure CdSe and MnCdSe solid solutions.

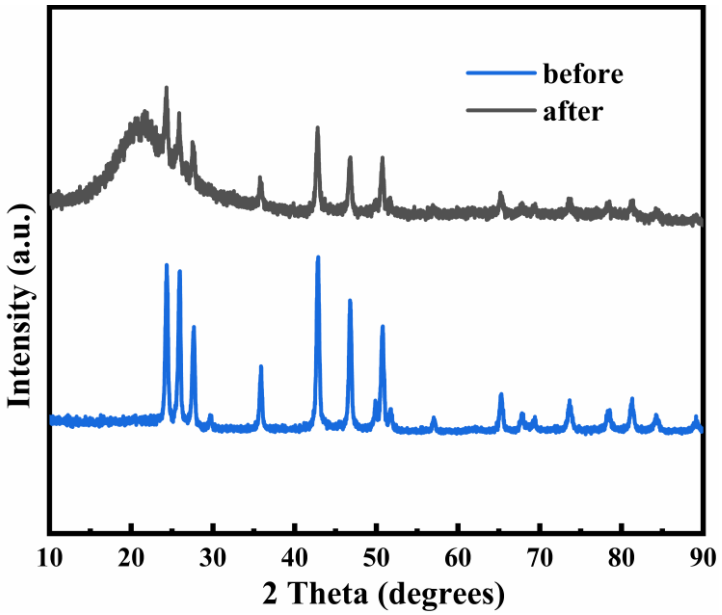

Fig. S8. XRD patterns of $Mn_{0.68}Cd_{0.32}Se_{1+x}$ before and after the photocatalytic cycle experiment. (Note: The peak at about 22° in the spent $Mn_{0.68}Cd_{0.32}Se_{1+x}$ can be ascribed to the characteristic peak of the quartz sample holder)

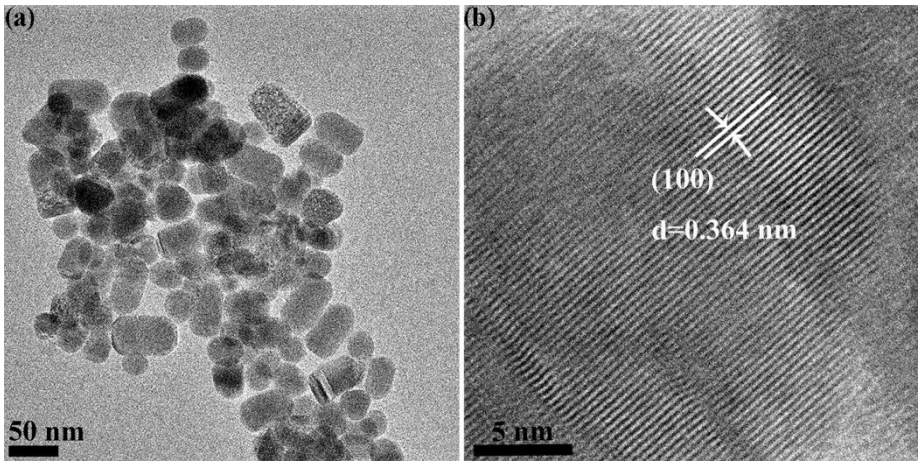

Fig. S9. TEM (a) and HRTEM images (b) of $Mn_{0.68}Cd_{0.32}Se_{1+x}$ after the cycled photocatalytic experiment.

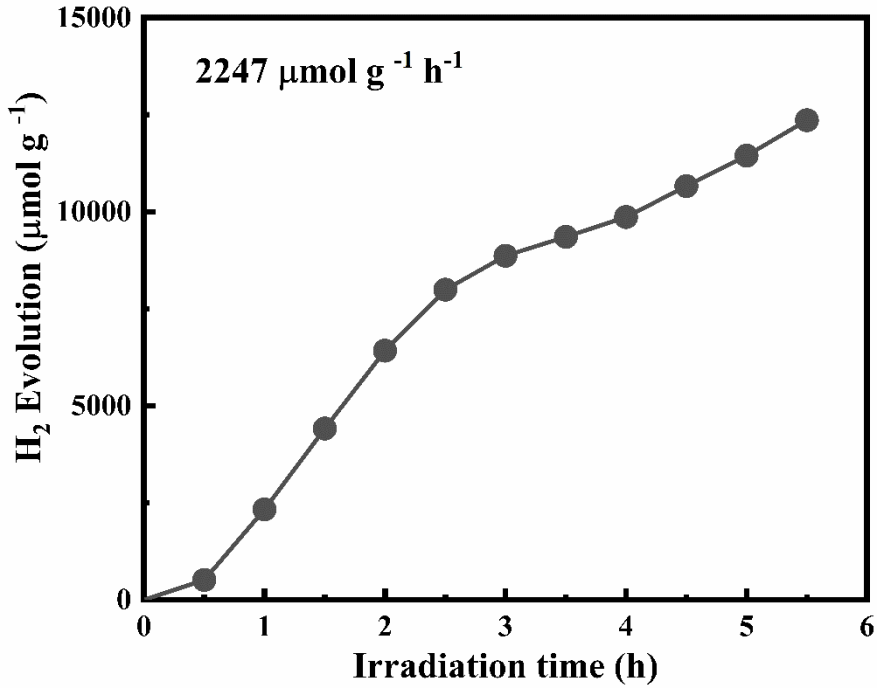

Fig. S10. Time course for photocatalytic H_2 production of the recycled $Mn_{0.68}Cd_{0.32}Se_{1+x}$ after 37 days.

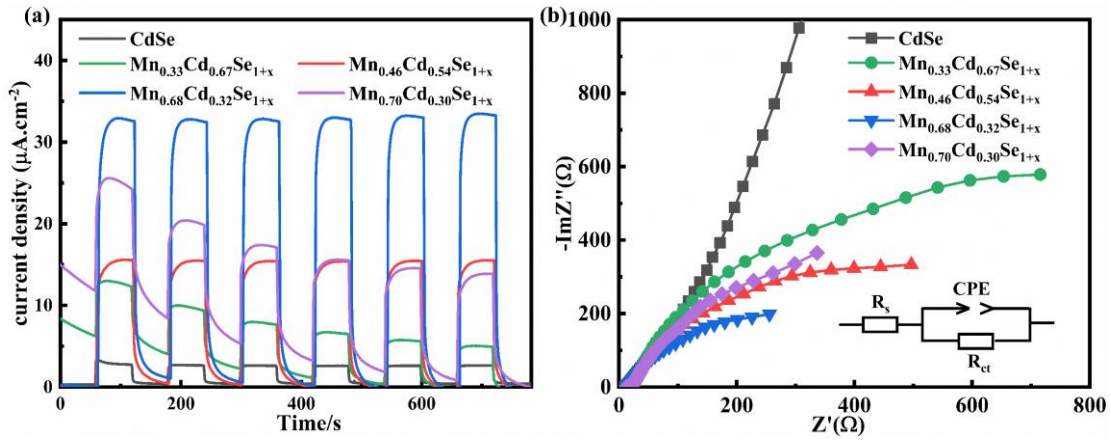

Fig. S11. (a) transient photocurrent responses and (b) EIS Nyquist plots (inset: equivalent circuit diagram) of pure CdSe, and MnCdSe solid solution.

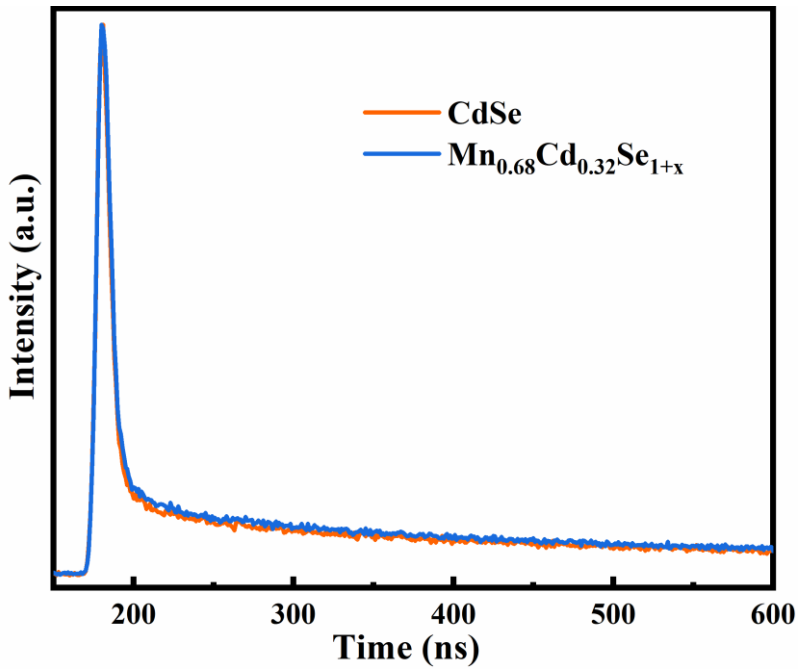

Fig. S12. Time-resolved photoluminescence (TRPL) spectra of CdSe, and $Mn_{0.68}Cd_{0.32}Se_{1+x}$.

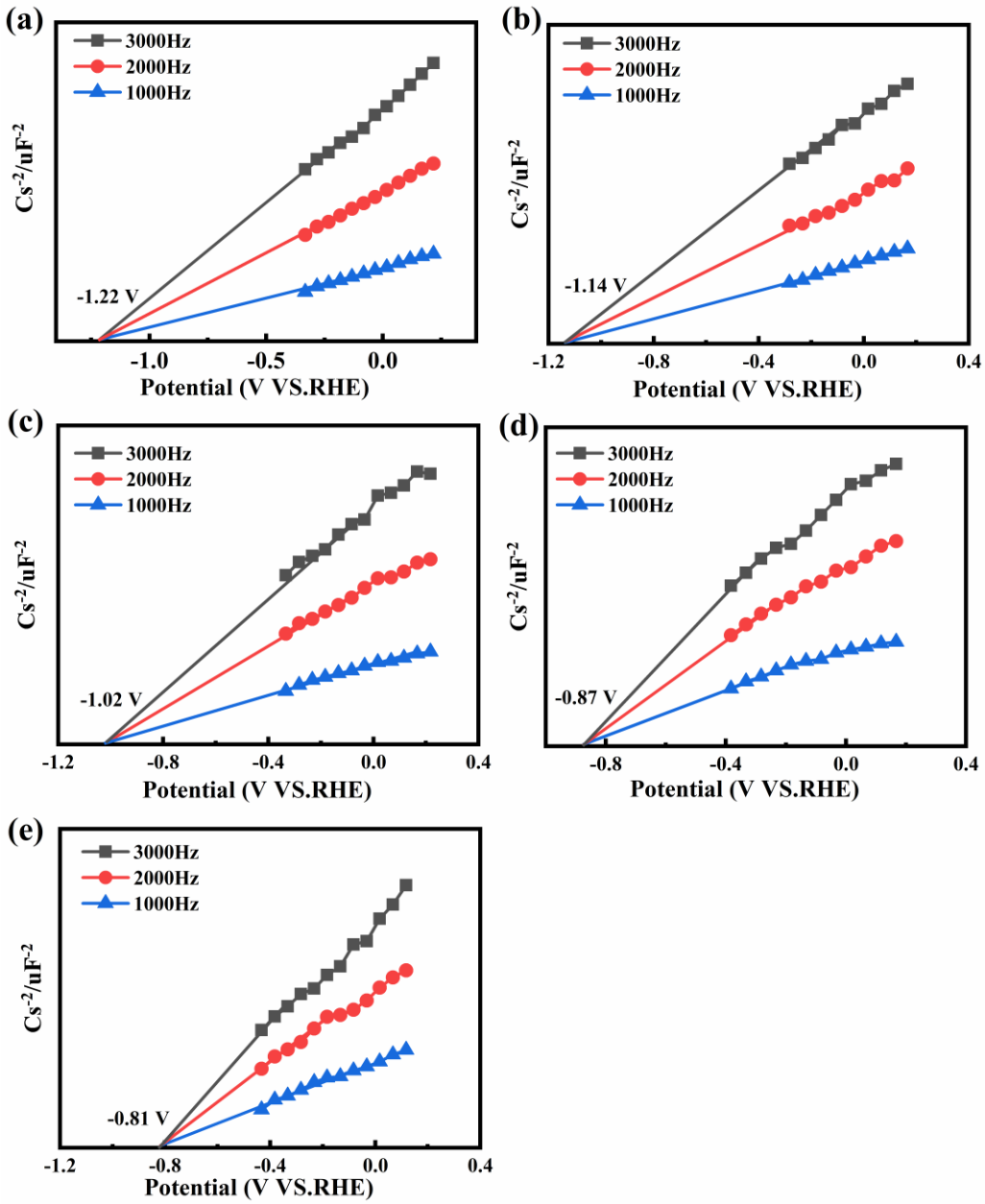

Fig. S13. Mott-Schottky plots of (a) CdSe, (b) $Mn_{0.33}Cd_{0.67}Se_{1+x}$, (c) $Mn_{0.46}Cd_{0.54}Se_{1+x}$, (d) $Mn_{0.68}Cd_{0.32}Se_{1+x}$, and (e) $Mn_{0.70}Cd_{0.30}Se_{1+x}$ samples.

Table. S1. The Mn/Cd/Se molar ratio in the MnCdSe solid solutions was determined by inductively coupled plasma-atomic emission spectroscopy (ICP-AES).

Samples	Precursor composition (mmol)			ICP-AES
	$MnCl_2$	$CdCl_2$	Se	Mn:Cd:Se
CdSe	0	3	3	0: 1: 1
$Mn_{0.33}Cd_{0.67}Se_{1+x}$	2.4	0.8	3	0.33: 0.67: (1+0.03)
$Mn_{0.46}Cd_{0.54}Se_{1+x}$	2.4	0.6	3	0.46: 0.54: (1+0.07)
$Mn_{0.68}Cd_{0.32}Se_{1+x}$	2.4	0.485	3	0.68: 0.32: (1+0.20)
$Mn_{0.70}Cd_{0.30}Se_{1+x}$	2.4	0.4	3	0.70: 0.30: (1+0.18)

Table. S2. Comparison of the photocatalytic H_2 evolution performance of the metal selenide photocatalysts.

Catalysts	Light Source	Sacrificial reagent	H_2 Evolution Rate ($\mu mol\ g^{-1}\ h^{-1}$)	AQY (%) (Wavelength)	Ref.
CdSe/ZnCr-LDH	300 W Xe lamp ($\lambda \geq 420$ nm)	Na_2S /Na_2SO_3	2196	---	3
In_2Se_3 NPS	300 W Xe lamp ($\lambda \geq 420$ nm)	Na_2S /Na_2SO_3	1347.59	---	4
ZnO-CdSe	300 W Xe lamp ($\lambda \geq 420$ nm)	Na_2S /Na_2SO_3	1045	---	5
$FeSe_2$/ZnSe	300 W Xe lamp	methanol	1228	4.1% (360 nm)	6
CdSe	275 W Xe lamp ($\lambda > 400$ nm)	Na_2S /Na_2SO_3	233	---	7
$Zn_{0.5}Cd_{0.5}Se$	300 W Xe lamp ($\lambda \geq 400$ nm)	Na_2S /Na_2SO_3	10 ($\mu mol\ h^{-1}$)	---	8
CdSe QDs	300 W Xe lamp ($\lambda \geq 420$ nm)	Na_2SO_3	630	---	9
CdSe	300 W Xe lamp ($\lambda \geq 400$ nm)	Na_2S /Na_2SO_3	1153	---	10
ZnSe	500 W Xe lamp ($\lambda > 420$ nm)	Ascorbic acid	330	---	11
ZnSe/ZnS	500 W Xe lamp ($\lambda > 420$ nm)	Ascorbic acid	1810	1.57% (420 nm)	11
CdSe	300 W Xe lamp ($\lambda > 420$ nm)	Na_2S /Na_2SO_3	6	---	12
ZnSe	300 W Xe lamp ($\lambda > 420$ nm)	Na_2S /Na_2SO_3	1056	---	12
$Zn_{0.5}Cd_{0.5}Se$	300 W Xe lamp ($\lambda \geq 420$ nm)	Na_2S /Na_2SO_3	438.3	1.7% (420 nm)	13
MnCdSe	**300 W Xe lamp ($\lambda > 420$ nm)**	**Na_2S /Na_2SO_3**	**2582**	**7.5% (420 nm)**	**This work**

Table. S3. Fitting results of the Nyquist plots for CdSe, and MnCdSe solid solution.

Photocatalyst	R_s (Ω)	R_{ct} (Ω)	CPE ($F \cdot cm^{-2} \cdot S^{n-1}$)	n
CdSe	16.55	21306	2.9E-3	0.78
$Mn_{0.33}Cd_{0.67}Se_{1+x}$	17.81	1852	1.2E-3	0.78
$Mn_{0.46}Cd_{0.54}Se_{1+x}$	16.63	1210	1.8E-3	0.74
$Mn_{0.68}Cd_{0.32}Se_{1+x}$	16.41	1146	4.1E-3	0.70
$Mn_{0.70}Cd_{0.30}Se_{1+x}$	17.65	1699	2.2E-3	0.78

Note: Rs is Ohm internal resistance, Rct represents the charge transfer resistance, and CPE is the constant phase element.

References

1. R. Abargues, J. Navarro, P. J. Rodriguez-Canto, A. Maulu, J. F. Sanchez-Royo and J. P. Martinez-Pastor, *Nanoscale*, 2019, **11**, 1978-1987.
2. W. Wang, T. Ding, G. Chen, L. Zhang, Y. Yu and Q. Yang, *Nanoscale*, 2015, **7**, 15106-15110.
3. G. Zhang, B. Lin, Y. Qiu, L. He, Y. Chen and B. Gao, *Int. J. Hydrogen Energy*, 2015, **40**, 4758-4765.
4. R. Wang, J. Wan, J. Jia, W. Xue, X. Hu, E. Liu and J. Fan, *Mater. Des.*, 2018, **151**, 74-82.
5. X. Wang, C. Zhou, W. Wang, B. Du, J. Cai, G. Feng and R. Zhang, *J. Alloy Compd.*, 2018, **747**, 826-833.
6. J. Zhang, P. Tian, T. Tang, G. Huang, J. Zeng, B. Cui, Z. Shen, H. Wang, Z. Kong, J. Xi and Z. Ji, *Int. J. Hydrogen Energy*, 2020, **45**, 8526-8539.
7. R. Bera, A. Dutta, S. Kundu, V. Polshettiwar and A. Patra, *J. Phys. Chem. C*, 2018, **122**, 12158-12167.
8. J. Y. Choi, K. M. Nam and H. Song, *J. Mater. Chem. A*, 2018, **6**, 16316-16321.
9. I. Grigioni, M. Bernareggi, G. Sinibaldi, M. V. Dozzi and E. Selli, *Appl. Catal., A*, 2016, **518**, 176-180.

10. A. Thibert, F. A. Frame, E. Busby, M. A. Holmes, F. E. Osterloh and D. S. Larsen, *J. Phys. Chem. Lett.*, 2011, **2**, 2688-2694.
11. Y. Feng, M. Xu, P.-L. Tremblay and T. Zhang, *Int. J. Hydrogen Energy*, 2021, **46**, 21901-21911.
12. L. Wei, D. Zeng, J. Liu, H. Zheng, T. Fujita, M. Liao, C. Li and Y. Wei, *J. Colloid Interface Sci.*, 2022, **608**, 3087-3097.
13. L. Wei, D. Zeng, X. He, L. Wang, Y. Bao, G. He, T. Fujita and W.-J. Ong, *Adv. Energy Sustainability Res.*, 2022, **n/a**, 2100210.